

**Few-cycle shock X-wave generation by filamentation in prealigned molecules**Jian Wu,<sup>1</sup> Hua Cai,<sup>1</sup> Arnaud Couairon,<sup>2</sup> and Heping Zeng<sup>1,\*</sup><sup>1</sup>*State Key Laboratory of Precision Spectroscopy, East China Normal University, Shanghai 200062, China*<sup>2</sup>*Centre de Physique Théorique, École Polytechnique, CNRS, F-91128 Palaiseau, France*

(Received 17 October 2008; published 28 July 2009)

We investigate the evolution of an intense femtosecond laser pulse in prealigned molecules of nitrogen following impulsive rotational Raman excitation by a weak pump pulse. The spatiotemporal and spectral dynamics of the probe pulse are readily controlled by matching the delay between pump and probe to various revivals of the molecular alignment. This control allows for intense filamentation of the probe and generation of self-shortened few-cycle pulses with angular spectra featuring shock X-waves. We identify the phase modulation originating from the sharp revivals of the molecular alignment as responsible for the generation of controllable rising or falling shock edges associated with on-axis redshifted or blueshifted supercontinuum spectrum and off-axis blueshifted or redshifted tails. Pulse self-steepening promotes the formation of the conical emission associated with the off-axis red tails, the blueshifted supercontinuum and the shock in the trailing part of the pulse.

DOI: [10.1103/PhysRevA.80.013828](https://doi.org/10.1103/PhysRevA.80.013828)

PACS number(s): 42.65.Re, 42.65.Sf, 42.65.Jx, 42.65.Tg

**INTRODUCTION**

Filamentation of ultrashort laser pulses was foreseen as a flexible source of secondary radiation [1]. For instance, supercontinuum and secondary infrared sources [2–6], few-cycle driving pulses for high-order harmonics and attosecond pulse generation [7–9], remote THz radiation [10,11], and subdiffractive conical -waves [12–16] are obtained spontaneously during optical filamentation. A control of this spontaneous generation would be highly desirable, which can be achieved by acting on the generation of optical shocks formed by the filament. Ultrashort laser pulses of near-femtosecond or subfemtosecond shocked fronts form spontaneously during the generation of powerful electromagnetic bubbles [17] or by cascaded stimulated Raman scattering [18]. Generally, in normally dispersive media, a rising shock in the leading part of the pulse is associated with a redshifted spectrum, while a falling shock in the trailing part of the pulse corresponds to a spectral blueshift with respect to the incident pulse [19,20]. Self-compressed few-cycle pulses generated at the end of intense femtosecond filamentation result from significant spatiotemporal reshaping and spectral broadening of the incident pulses intrinsically linked to optical shocks [7,21]. By using a molecular gas, the dynamics of ultrashort laser pulses undergoing filamentation and the features of the resulting pulse can be controlled since the relative orientation of the molecule to the field polarization can be manipulated by impulsive rotational Raman excitation with periodic revivals [22]. Field-free molecular alignment has been extensively studied for full-dimensional molecular manipulation [23], molecular-orbital reconstruction [24], ultrashort pulse compression [25], high-harmonic generation [26,27], probe pulse focusing and spectral modulation [28], few-cycle ultrashort laser-pulse tuning [29], and very recently for filamentation [5,6,30,31] and associated pulse compression [32].

In this paper, we numerically investigate the evolution of an intense ultrashort probe pulse in nitrogen molecules during the revivals of molecular alignment following impulsive rotational Raman excitation by a weak collinearly propagating pump pulse. We show that intense filamentation of the probe pulse is controlled by properly matching it to the revivals of the impulsive molecular alignment, leading to the generation of few-cycle shock X-waves.

**ANALYSIS OF THE EFFECTS OF MOLECULAR ALIGNMENT ON INTENSE LASER PULSES**

The effect of the molecular alignment on the probe pulse  $E(r,t)$  can be inferred from the space-time-dependent frequency shift  $\delta\omega(r,t) \propto -(\partial/\partial t)[n_2|E(r,t)|^2 + \delta n(r,t)]$ , where  $n_2 = 2.3 \times 10^{-19} \text{ cm}^2/\text{W}$  denotes the nonlinear refractive index of nitrogen. The second term  $\delta n(r,t) = 0.5(\rho_0 \Delta\alpha/n_0)[\langle \cos^2 \theta(r,t) \rangle - 1/3] + \delta n_{rR}(r,t)$  extends the standard theory of self-phase-modulation (SPM) and accounts for the contribution of the molecular alignment, where  $\rho_0 = 2.5 \times 10^{19} \text{ cm}^{-3}$  is the initial molecular density,  $\Delta\alpha = \alpha_{\parallel} - \alpha_{\perp}$  is the polarizability difference [22], and  $n_0$  is the linear refractive index. The rotational Raman contribution  $\delta n_{rR}$  of the pre-excited molecules to the nonlinear index is modeled as in Ref. [33] and effectively depends on the pump intensity. During the pump excitation with electric field  $E_{\text{pump}}(t)$ , the evolution of the molecular rotational state  $|\psi\rangle = \sum_{JM} C_{JM} |JM\rangle$  is calculated by integrating the time-dependent Schrödinger equation  $i\hbar \partial|\psi\rangle/\partial t = H_0|\psi\rangle$  for each initial state  $|\psi(t=0)\rangle_{J_0M_0} = |J_0M_0\rangle$  by using the fourth-order Runge-Kutta method, where  $H_0 = B_0J(J+1) + D_0J^2(J+1)^2 - 1/4\Delta\alpha E_{\text{pump}}^2(t)\cos^2\theta$  is the effective Hamiltonian where  $B_0$  and  $D_0$  are the rovibrational molecular constants [22,34]. The molecular alignment degree  $\langle \cos^2 \theta(t) \rangle$  is then obtained as an ensemble average of all contributions  $\langle \cos^2 \theta(t) \rangle_{J_0M_0} = \langle \psi(t)|_{J_0M_0} \cos^2 \theta |\psi(t)\rangle_{J_0M_0}$  by assuming a temperature-dependent Boltzmann distribution of the initial molecular states  $|J_0M_0\rangle$ . Periodic field-free molecular alignment revivals after the extinction of the pump pulse result from the

\*Corresponding author; hpzeng@phy.ecnu.edu.cn

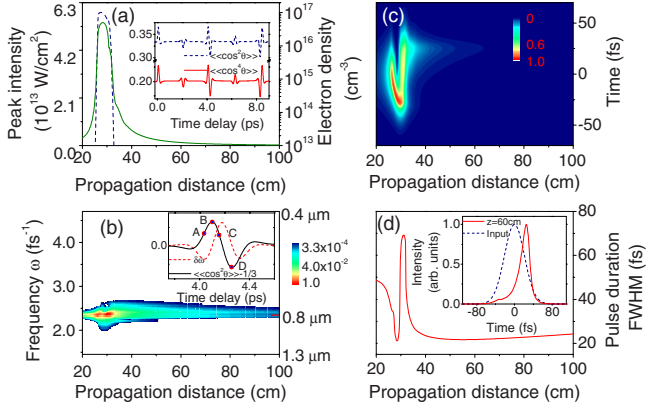


FIG. 1. (Color online) Spatiotemporal evolution of the probe pulse without molecular alignment. (a) Peak intensity (solid curve) and electron density (dashed curve), (b) on-axis spectral profile (log scale), (c) on-axis temporal profile (linear scale), (d) on-axis pulse duration of the probe pulse versus propagation distance. The time-dependent alignment metrics, the frequency shifts induced by the molecular alignment revivals, and the on-axis temporal profiles of the probe pulse at  $z=0$  and 60 cm are presented in the insets of (a), (b), and (d), respectively. Without pump,  $\langle\langle\cos^2 \theta\rangle\rangle=1/3$  and  $\langle\langle\cos^4 \theta\rangle\rangle=1/5$  [inset of 1(a)].

periodic beatings of the pre-excited rotational wave packets.

We start with a simple analysis of the expected effects of cross-phase-modulation (XPM) induced by the revival of molecular alignment on the probe pulse. The inset of Fig. 1(a) shows the time-dependent molecular alignment metrics for nitrogen with  $\Delta\alpha=10^{-30}$  m<sup>3</sup> and a pump intensity of  $2 \times 10^{13}$  W/cm<sup>2</sup>. As shown in the inset of Fig. 1(b), the probe pulse will experience spectral redshift or blueshift depending on whether its temporal peak is delayed to the rising or falling edge of the molecular alignment revival, which is proportional to  $-(\partial/\partial t)[\langle\langle\cos^2 \theta(t)\rangle\rangle-1/3]$ . The pulse spectrum is further broadened as a result of SPM. In normally dispersive media, red frequency components propagate faster than the blue ones. When the probe pulse experiences the falling edge of the molecular alignment revival, redder frequencies in the less intense rising part of the pulse will be diffracted by the molecular gas and eventually form redshifted conical emission, while new bluer frequencies originating from SPM and XPM induced by the revival of molecular alignment [see the inset of Fig. 1(a)] will enhance the falling shock in the trailing edge of the pulse. This will result in a wave packet with a broadband blueshifted axial spectrum, redshifted conical emission, and a falling shock in the trailing part, i.e., a shock X-wave [20]. In contrast, a blueshifted conical emission associated with a redshifted axial spectrum and a rising shock in the leading part of the pulse is expected when the probe pulse experiences the rising edge of the molecular alignment revival.

### MODELING OF PULSE PROPAGATION IN PREALIGNED MOLECULES

In order to test the possible formation of shock X-waves in a molecular alignment revival, we numerically solved the

nonlinear envelope equation governing the propagation of the probe pulse  $E(z, r, t)$  in prealigned nitrogen molecules,

$$\begin{aligned} \frac{\partial E}{\partial z} = & \frac{i}{2k_0} T^{-1} \frac{1}{r} \frac{\partial}{\partial r} \left( r \frac{\partial E}{\partial r} \right) - i \frac{k_0^{(2)}}{2} \frac{\partial^2 E}{\partial t^2} + \frac{k_0^{(3)}}{6} \frac{\partial^3 E}{\partial t^3} \\ & + ik_0 T \left[ \delta n(z, r, t) + \frac{n_2}{n_0} |E|^2 \right] E - T^{-1} \frac{\sigma}{2} (1 + i\omega_0 \tau_c) \rho E \\ & - \frac{\beta_K}{2} |E|^{2K-2} \left( 1 - \frac{\rho}{\rho_0} \right) E. \end{aligned} \quad (1)$$

Here, cylindrical symmetry is assumed with  $r \equiv \sqrt{x^2 + y^2}$ ,  $k_0 = n_0 \omega_0 / c$  is the wave number of the probe pulse at carrier frequency  $\omega_0$ , and  $k_0^{(2)} = 0.2$  fs<sup>2</sup>/cm and  $k_0^{(3)} = 0.1$  fs<sup>3</sup>/cm are the second- and third-order dispersion coefficients. The model includes XPM induced by the molecular alignment revival in the refractive index change  $\delta n(z, r, t)$ , the Kerr effect with coefficient  $n_2 = 2.3 \times 10^{-19}$  cm<sup>2</sup>/W, plasma defocusing and inverse Bremsstrahlung with collision time  $\tau_c = 350$  fs and cross section  $\sigma = 5.4 \times 10^{-20}$  cm<sup>2</sup>, and multiphoton absorption with cross section  $\beta_K$ . Extending our previous model [32], the operator  $T \equiv 1 + i\omega_0^{-1} \partial/\partial t$  accounts for space-time focusing and self-steepening of the pulse [1]. The evolution of the electron density  $\rho(z, r, t)$  is calculated by resolving  $\partial\rho/\partial t = \sigma_K |E|^{2K} (\rho_0 - \rho)$  at each propagation step with  $K=11$ . The orientation-dependent cross section for multiphoton ionization  $\sigma_K = \beta_K / (K\hbar\omega_0\rho_0)$  is modeled by  $\sigma_K = \sigma_{K0} [1 + (1.5a_2 - 3.75a_4)(\langle\langle\cos^2 \theta\rangle\rangle - 1/3) + 4.375a_4(\langle\langle\cos^4 \theta\rangle\rangle - 1/5)]$ , where the coefficients  $a_2 = 0.39$  and  $a_4 = -0.21$  for N<sub>2</sub> are taken from Ref. [26] and  $\sigma_{K0} = 6.31 \times 10^{-140}$  s<sup>-1</sup> cm<sup>22</sup>/W<sup>11</sup> accounts for the ionization cross section of randomly oriented nitrogen molecules [35]. The dependence of the pump intensity on radial and longitudinal coordinates  $r$  and  $z$  is responsible for the  $r$  and  $z$  dependences of the refractive index change  $\delta n(z, r, t)$  and the alignment signals  $\langle\langle\cos^2 \theta(z, r, t)\rangle\rangle$  and  $\langle\langle\cos^4 \theta(z, r, t)\rangle\rangle$ , the time dependence of which is precalculated from the evolution of the pump electric field and its introduction in the Hamiltonian  $H_0$ , as indicated above. The collinearly propagating pump and probe pulses at 800 nm are assumed to have the same polarization, beam diameter of 1.5 mm, pulse duration of 50 fs, and are focused by the same lens ( $f = 30$  cm unless otherwise specified). The input peak power of the probe pulse is  $P_{in} = 2P_{cr}$ , where  $P_{cr} = 4.4$  GW is the critical power for self-focusing at 800 nm in N<sub>2</sub> at 1 atm. We checked by numerically propagating the pump pulse ( $P_{pump} = 1.1$  GW) in randomly orientated nitrogen molecules that its propagation can be assumed to obey the laws of Gaussian optics. The maximum ionization degree of molecular nitrogen around the geometric focus of the lens was calculated to be  $\sim 6.5 \times 10^{-7}$  (data not shown). The plasma generated by the pump has thus negligible influence on the succeeding propagation of the probe pulse. In the following discussion, the probe pulse is tuned to various delays (labeled as A, B, C, and D) around the half revival of the molecular alignment as shown in the inset of Fig. 1(b).

## RESULTS OF NUMERICAL SIMULATIONS

Figure 1 shows the spatiotemporal evolution of the probe pulse when the nitrogen molecules are randomly oriented, i.e., when the pump pulse is turned off. This constitutes our reference case characterized by short ( $\sim 7$  cm) plateaus of the maximum intensity and electron density [Fig. 1(a)] in the filament, and limited spectral broadening [Fig. 1(b)]. Figure 1(c) shows the refocusing dynamics of the pulse: the generated plasma pushes the self-focused probe pulse toward its leading edge until the end of the intensity plateau is reached [7,36]. The refractive index seen by the trailing part of the pulse is lowered by the electron plasma generated by the leading part of the pulse. During the early stage of filamentation ( $25 < z < 30$  cm), the intensity distribution of the pulse trail is defocused. Around the geometric focus of the lens ( $30 < z < 32$  cm), the off-axis light is refocused. However, Fig. 1(c) shows that the pulse is at the verge of initiating a second complete refocusing cycle that would lead to a motion of the trailing peak toward the leading edge. Beyond the refocusing point, filamentation stops, the electron density decreases [Fig. 1(a)], and the pulse propagates almost linearly over several tens of centimeters with a stable duration of  $\sim 22$  fs [Fig. 1(d)]. The inset of Fig. 1(d) presents a comparison of the temporal profile of the pulse at a propagation distances of  $z=0$  and  $z=60$  cm.

When the pump pulse is turned on, the filamentation dynamics is controlled by the spatiotemporal XPM from the revival of the molecular alignment, which induces not only an additional spectral modulation similar to SPM, but also an associated focusing or defocusing effect. Due to the Gaussian-shaped transverse profile of the pump pulse, molecular alignment is indeed more significant in the beam center than in its periphery thus, focusing is enhanced when molecular orientation is parallel to the field polarization, or reduced when it is perpendicular. To make it tractable, the analysis of XPM induced by aligned molecules presented above did not include the effect of self-steepening. We therefore discuss first simulation results shown in Figs. 2 and 3 obtained with the approximation  $T \approx 1$  in Eq. (1) and then discuss the effect of self-steepening on the results in Figs. 4–6.

## RESULTS WITHOUT SELF-STEEPENING

Figure 2 shows the evolution of the probe pulse as its temporal peak is tuned to the rising edge of the molecular alignment revival (delay A). The filamentation length reaches  $\sim 50$  cm [Fig. 2(a)] for the parallel molecular orientation with  $\langle \langle \cos^2 \theta \rangle \rangle > 1/3$ , which enhances focusing of the probe pulse. This represents a considerable increase with respect to the case of the absence of pump pulse. As predicted from the above-mentioned analysis of phase modulation, the spectrum of the probe pulse is significantly broadened with a maximum of redshifted frequency components due to the strong phase modulation from the rising edge of the molecular alignment revival [Fig. 2(b)]. Figure 2(c) shows that around the geometric focus of the lens, the trail of the probe pulse experiences a much stronger refocusing in aligned molecules than in the case of randomly oriented molecules. During the

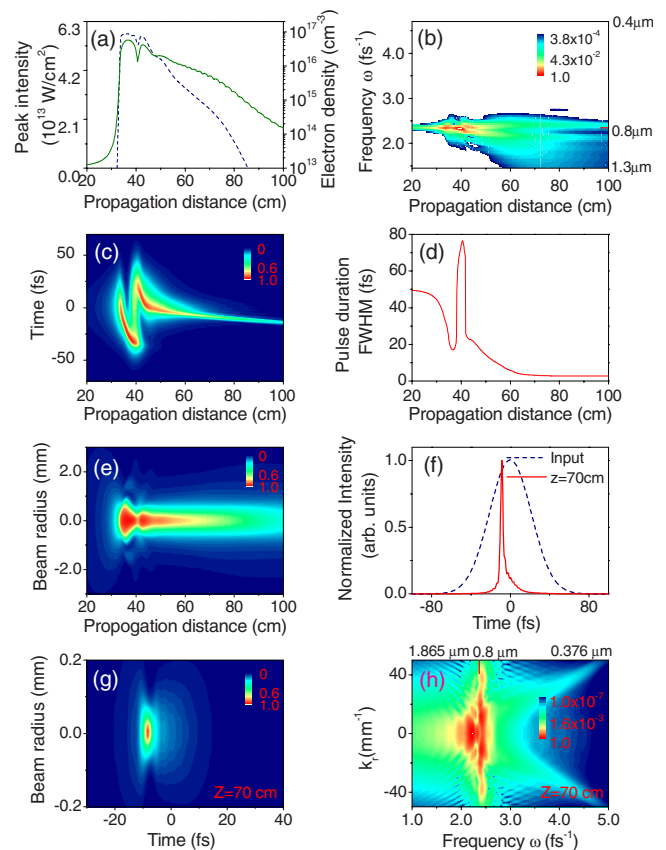


FIG. 2. (Color online) Spatiotemporal evolution of the probe pulse when it is tuned to match the molecular alignment revival at delay A. (a) Peak intensity (solid curve) and electron density (dashed curve), (b) on-axis spectral profile (log scale), (c) on-axis temporal profile (linear scale), (d) on-axis pulse duration, (e) spatial profile (linear scale) of the probe pulse versus propagation distance. (f) On-axis temporal profiles, (g) near-field (linear scale), and (h) far-field (log scale) intensity distributions of the probe pulse at  $z = 70$  cm. Here, self-steepening is not included in Eq. (1), and the probe pulse is focused with a lens of  $f = 40$  cm.

refocusing stage, the probe pulse accelerates and gradually advances in the negative side of the time-axis, in agreement with a previous report of this effect [19]. The pulse is further self-compressed to a temporal duration of  $\sim 3$  fs and propagates in the form of a few-cycle pulse over a distance of several tens of centimeters [Fig. 2(d)]. Although plasma defocusing plays a significant role in the shortening process, the enhancement of redder frequency components makes the temporal compression scenario slightly different from that usually obtained with filaments in gases [7,36–38], where the self-compressed pulse is most usually obtained in the trailing part and associated with a supercontinuum extending toward the blue side. Here the on-axis temporal profile of the probe pulse at  $z = 70$  cm plotted in Fig. 2(f) exhibits a rising shock edge. Figure 2(g) show the intensity distribution of this few-cycle wave packet which corresponds to the formation of an X-shaped angular spectrum [Fig. 2(h)] during intense filamentation. The X-shaped angular spectrum exhibits on-axis redshifted supercontinuum and blueshifted conical tails which feature conical emission with different frequencies

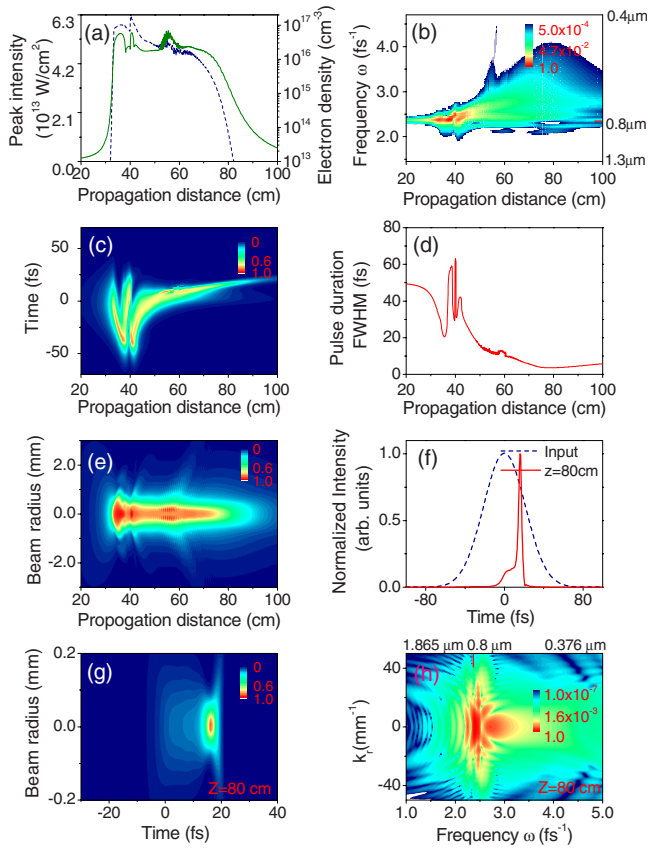


FIG. 3. (Color online) Same presentation and simulation parameters as in Fig. 2 but for the probe matching the molecular alignment revival at delay C.

propagating at different angles [12–14,39]. The structure of this wave packet was formerly identified in condensed media as a shock X-wave [20]. Since condensed media have a much stronger dispersion, the formation of shock X-waves does not crucially depend on the medium. Similarly, Ref. [20] and results below show that such structures are still formed in the presence of self-steepening. The molecular alignment allows for a control of the filamentation dynamics which leads to few-cycle shock X-waves propagating over more than 40 cm with a preserved  $\sim 3$  fs pulse duration [Fig. 2(c)], a slowly decreasing peak intensity [Fig. 2(a)], and a slightly broadening beam width [Fig. 2(e)].

Figure 3 shows the detailed evolution of the probe pulse obtained for the same parameters except that its temporal peak is tuned to the falling edge of the molecular alignment revival (delay C). A filament of  $\sim 50$  cm is generated with an almost constant peak intensity and beam width [FWHM of the fluence distribution as shown in Fig. 3(e)]. The on-axis peak intensity, and on-axis electron density versus the propagation distance are shown in Fig. 3(a). Due to the significant phase modulation in the falling edge of the molecular alignment revival, the spectrum is considerably broadened in the blue side [Fig. 3(b)]. As shown in Fig. 3(c), refocusing of the probe pulse becomes significant for the leading part rather than the trailing part, after a transient refocusing of the trailing part. This is due to the fact that for delays matching the falling-off of the molecular alignment revival, the leading

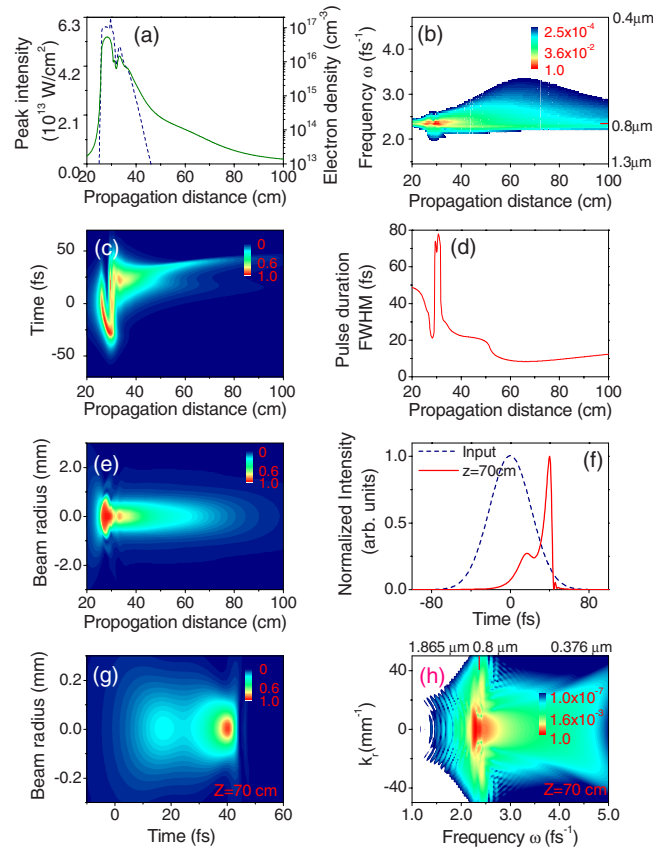


FIG. 4. (Color online) Same presentation and simulation parameters as in Fig. 2 (delay A), but self-steepening is included in Eq. (1) and the probe pulse is focused with a lens of  $f=30$  cm.

part of the probe pulse sees a larger positive lens effect than its trail, therefore refocusing of the probe pulse finally becomes significant for the leading part. The refocused pulse is then gradually delayed to the trailing part of the pulse due to the efficient generation of new blue frequencies and the normal dispersion of the medium. Thus, molecular alignment counteracts the effect of self-generated plasma which would have maintained the pulse in the leading part. Figure 3(d) presents the evolution of the duration of the probe pulse versus the propagation distance. The probe pulse is compressed down to  $\sim 3.7$  fs after significant spatiotemporal reshaping during intense filamentation. The on-axis temporal profile of the self-compressed probe pulse at  $z=80$  cm is plotted in Fig. 3(f), which shows a fairly sharp falling shock edge in the pulse trail. As predicted from the analysis of phase modulation and confirmed in Figs. 3(g) and 3(h), a few-cycle shock X-wave is also generated for delay C, but in contrast with delay A, it has a falling edge. The X-shaped angular spectrum shown in Fig. 3(h), exhibits on-axis blue-shifted supercontinuum and redshifted conical tails. The redshifted conical tails are interpreted as resulting from the excitation of the redder frequency components in the leading part of the probe pulse [Fig. 3(c)] and their subsequent diffraction while they travel faster than the initial group velocity  $v_g(\omega_0)$  of the wave packet to reach the region of weak intensities ahead the peak of the pulse.

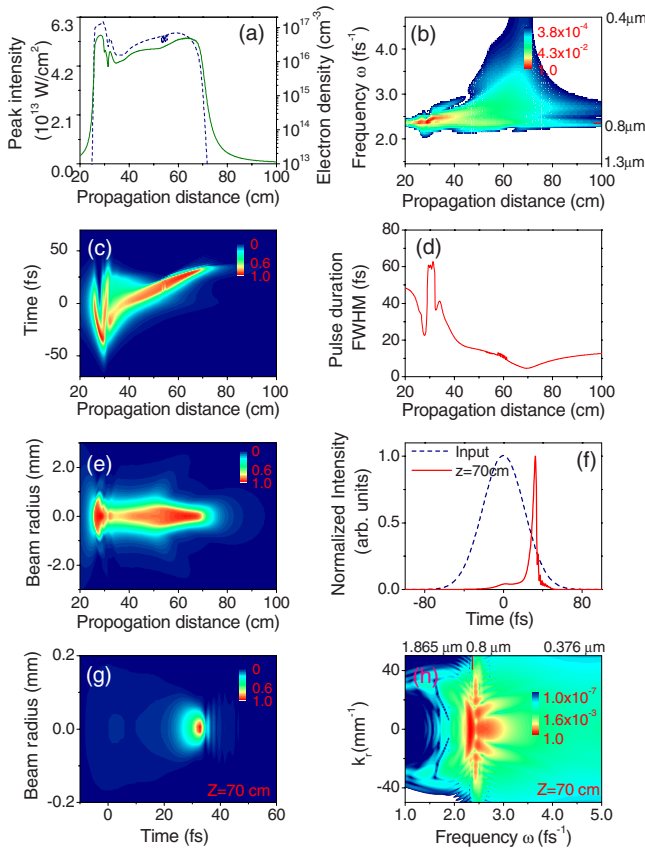


FIG. 5. (Color online) Same presentation and simulation parameters as in Fig. 4 but for the probe matching the molecular alignment revival at delay C.

### RESULTS WITH SELF-STEEPENING

The fact that molecular alignment allows for longer filaments to be generated and the probe pulse to be reshaped into few-cycle shock X-waves is a generic result. When we consider the full model of Eq. (1) with self-steepening the result also holds with only slight changes which we now discuss. Figure 4 shows the filamentation and shock X-wave formation dynamics for the complete model of Eq. (1) including self-steepening when the temporal peak of the probe pulse is tuned to the rising edge of the molecular alignment revival (delay A). Comparison with Fig. 2, Fig. 4(e) shows that a  $\sim 50$  cm long filament is also obtained with nearly constant peak intensities [Fig. 4(a)] and leads to the formation of a few-cycle shock X-wave [Fig. 4(g)]. On the side of the differences, rather than the expected redshifted supercontinuum, the spectrum is considerably broadened in the blue side as shown in Fig. 4(b). Figure 4(c) shows that around the geometric focus of the lens, the trail of the probe pulse experiences a stronger refocusing than in the absence of self-steepening. Self-steepening therefore prevents the acceleration of the refocused pulse toward the leading edge. The probe pulse is further self-compressed to a temporal duration of  $\sim 8.5$  fs [Fig. 4(d)], which is slightly longer than in the simulation without self-steepening. The on-axis temporal profile of the probe pulse at  $z=70$  cm is plotted in Fig. 4(f) and shows a falling shock edge in the pulse trail with a

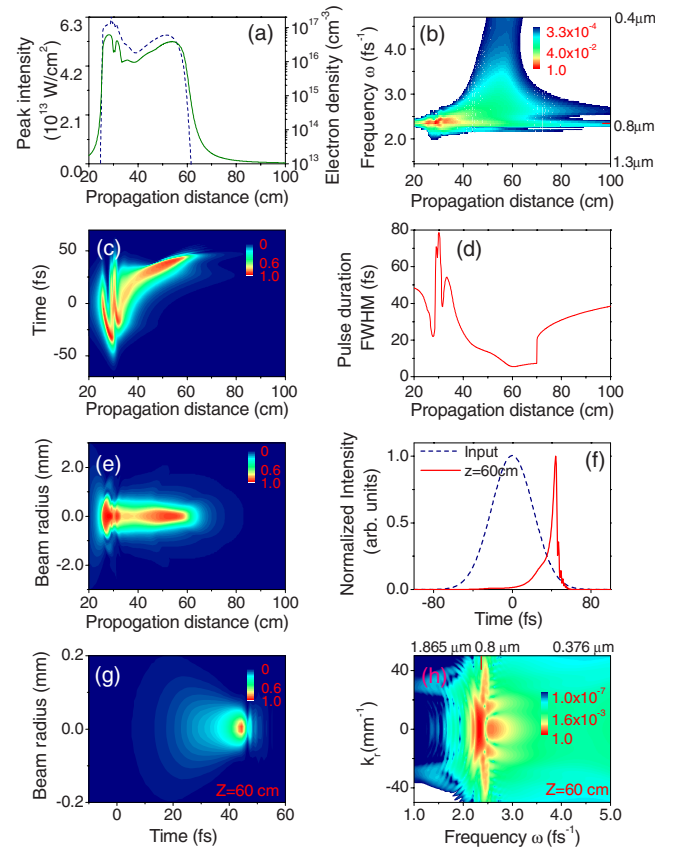


FIG. 6. (Color online) Same presentation and simulation parameters as in Fig. 4 but for the probe matching the molecular alignment revival at delay B.

noticeable spectral blueshift as in the case of molecular alignment revival at delay C. The intensity distribution in space and time of this profile is shown in Fig. 4(g) and corresponds to a few-cycle shock X-wave with features shown in Fig. 4(h). This wave packet dominates the filamentation dynamics and leads to gradually decreasing peak intensity and weak ionization along the propagation distance as shown in Figs. 4(a) and 4(e). Figure 5 finally shows that a few-cycle shock X-wave with a falling shock edge [Fig. 5(g)] is also generated when the temporal peak of the probe pulse is tuned to the falling edge of the molecular alignment revival (delay C). In this case, the result is fully in agreement with the analysis of phase modulation although the latter was made without considering self-steepening. By comparing Figs. 3 and 5, it is observed that the minimum duration of the probe pulse during its intense filamentation is slightly longer with self-steepening ( $\sim 4.6$  fs) [Fig. 5(d)] than without, but this does not prevent self-compressed filaments to reach the sub-cycle regime for possibly different parameters [40,41]. The pulse remains few-cycle over a shorter distance of a few centimeters and exhibits all other features of a shock X-wave with a falling shock edge [Figs. 5(f) and 5(g)] and a on-axis blueshifted supercontinuum [Fig. 5(b)] as well as redshifted conical tails [Fig. 5(h)].

The strongest self-focusing effect is observed for delay B (maximum parallel molecular alignment revival) and the results obtained in this case are summarized in Fig. 6. The

nonlinear focus is obtained at a shorter distance and a filament of  $\sim 37$  cm is generated [Figs. 6(a) and 6(e)]. This also leads to a few-cycle X-shaped wave of  $\sim 5.6$  fs with a falling shock edge in the pulse tail, as shown in Figs. 6(d) and 6(f)–6(h). Finally, when the temporal peak of the probe pulse is tuned to a perpendicular revival of molecular alignment (for instance delay  $D$  for which the probe pulse undergoes an additional defocusing effect from the perpendicular molecular orientation with  $\langle\langle\cos^2\theta\rangle\rangle < 1/3$ ), no filament is generated, and the probe pulse diffracts immediately after the geometric focus of the lens.

## DISCUSSION

We emphasize that molecular alignment allows for a control of the formation of shock X-waves rather than a determination of the distance at which these structures are formed. Shock X-waves were shown to appear spontaneously during real experiments of filamentation in water on the rising edge of the pulse with an on-axis redshifted supercontinuum and blueshifted conical tails, as well as on the falling edge of the pulse with on-axis blueshifted supercontinuum and redshifted conical tails [20]. In this case, rising or falling shock X-waves were shown to appear at different distances but self-steepening and the dispersion of water did not introduce a sufficient asymmetry between the leading and trailing parts of the pulse to prevent the rising shock X-wave to be formed. Another publication by Porras *et al.* [42] interpreted shock X-waves as due to spatiotemporal modulational instability of spatially localized structures such as Townes solutions resulting from beam self-focusing and collapse during filamentation [43]. Since modulational instability is not affected by uneven dispersive orders [44], this process leads symmetrically to rising and falling shock X-waves. Our simulations of filamentation in prealigned molecules showed that tuning the delay allowed for a selection of either the leading or the trailing shock X-wave during the generation process; however self-steepening introduces an asymmetry in the spectral broadening associated with shock X-waves, which counteracts the XPM induced by the rising edge of the revival of molecular alignment. Therefore, generating a rising shock X-wave may require an enhancement of the amplitude of the refractive index change due to molecular alignment which can be typically obtained by reducing the temperature of the gas. We finally note that this asymmetry is in keeping with the recent demonstration that self-steepening plays a significant role to broaden the spectra of ultrashort laser pulses in the blue side, an effect shown to be controllably enhanced by the molecular alignment revivals [5,6].

Recent measurements on two beam coupling between filament-forming beams in air demonstrated that an amplification of one of the intersecting beam could occur at the energy expense of the other by adjusting the relative delay

[45]. This led to a control of the filament conical emission which could be enhanced or suppressed by the interaction. Although the investigated delays were in the range of a few tens of fs corresponding to an overlap in time of the two pulses, the physical mechanism at the origin of the suppression of conical emission was shown to be the Raman rotational contribution to the Kerr effect induced by molecular alignment. Recently, conical emission accompanying filamentation has been revisited and interpreted as due to the generation of X waves in a number of publications [13–16,46], a phenomenon which is associated with beam self-cleaning [4,46]. Our simulations in conjunction with these publications are perfectly in keeping with the results by Bernstein *et al.* [45] and even suggest that conical emission accompanying filamentation, as a signature of the generation of shock X-waves, could be enhanced or suppressed by the use of a pump beam aligning the diatomic molecules of air prior propagation of the probe pulse. Even if the probe pulse was not sufficiently intense to form a filament by itself in randomly aligned molecules, it could generate a shock X-wave and thus lead to conical emission if it was properly delayed to match the revival of molecular alignment with parallel orientation. In contrast, a delay corresponding to perpendicular orientation would lead to the possible suppression of conical emission even for a probe pulse sufficiently powerful to form a filament by itself in randomly aligned molecules.

## CONCLUSIONS

In summary, we showed that self-compressed few-cycle shock X-waves with stable temporal duration over a quite long distance can be generated by properly delaying an intense ultrashort laser pulse to match the molecular alignment revivals. Since the generation of these few-cycle shock X-waves takes advantage of XPM induced by the revivals of molecular alignment, the filamentation regime can be reached for a lower power than that typically required with an atomic gas or a molecular gas without pre-alignment [16] and might even occur below the collapse threshold [47]. It may lead to extensive applications in various fields, such as high-harmonic generation [8,9], forward THz generation [10,11], beam cleaning [46], and filamentation nonlinear optics [4].

This work was funded in part by National Natural Science Fund (Grants No. 10525416 and No. 10804032), National Key Project for Basic Research (Grant No. 2006CB806005), Projects from Shanghai Science and Technology Commission (Grant Nos. 08ZR1407100 and 09QA1402000), Program for Changjiang Scholars and Innovative Research Team in University, and Shanghai Educational Development Foundation (Grant No. 2008CG29).

- [1] A. Couairon and A. Mysyrowicz, *Phys. Rep.* **441**, 47 (2007).
- [2] J. Kasparian *et al.*, *Opt. Lett.* **25**, 1397 (2000).
- [3] F. Théberge, N. Aközbek, W. Liu, A. Becker, and S. L. Chin, *Phys. Rev. Lett.* **97**, 023904 (2006).
- [4] S. L. Chin, F. Théberge, and W. Liu, *Appl. Phys. B: Lasers Opt.* **86**, 477 (2007).
- [5] H. Cai *et al.*, *Opt. Express* **17**, 5822 (2009).
- [6] J. Wu, H. Cai, Y. Peng, and H. Zeng, *Phys. Rev. A* **79**, 041404(R) (2009).
- [7] A. Couairon *et al.*, *J. Mod. Opt.* **53**, 75 (2006).
- [8] H. S. Chakraborty *et al.*, *Opt. Lett.* **31**, 3662 (2006).
- [9] A. Couairon, H. S. Chakraborty, and M. B. Gaarde, *Phys. Rev. A* **77**, 053814 (2008).
- [10] C. D'Amico *et al.*, *New J. Phys.* **10**, 013015 (2008).
- [11] C. D'Amico, A. Houard, M. Franco, B. Prade, A. Mysyrowicz, A. Couairon, and V. T. Tikhonchuk, *Phys. Rev. Lett.* **98**, 235002 (2007).
- [12] D. Faccio, A. Matijosius, A. Dubietis, R. Piskarskas, A. Varanavicius, E. Gaizauskas, A. Piskarskas, A. Couairon, and P. Di Trapani, *Phys. Rev. E* **72**, 037601 (2005).
- [13] D. Faccio *et al.*, *Opt. Commun.* **265**, 672 (2006).
- [14] A. Couairon, E. Gaizauskas, D. Faccio, A. Dubietis, and P. Di Trapani, *Phys. Rev. E* **73**, 016608 (2006).
- [15] D. Faccio, M. A. Porras, A. Dubietis, F. Bragheri, A. Couairon, and P. Di Trapani, *Phys. Rev. Lett.* **96**, 193901 (2006).
- [16] D. Faccio *et al.*, *Opt. Express* **16**, 1565 (2008).
- [17] A. E. Kaplan and P. L. Shkolnikov, *Phys. Rev. Lett.* **75**, 2316 (1995).
- [18] A. E. Kaplan, *Phys. Rev. Lett.* **73**, 1243 (1994).
- [19] A. L. Gaeta, *Phys. Rev. Lett.* **84**, 3582 (2000).
- [20] F. Bragheri, D. Faccio, A. Couairon, A. Matijosius, G. Tamosauskas, A. Varanavicius, V. Degiorgio, A. Piskarskas, and P. Di Trapani, *Phys. Rev. A* **76**, 025801 (2007).
- [21] S. Akturk *et al.*, *Opt. Express* **16**, 17626 (2008).
- [22] H. Stapelfeldt and T. Seideman, *Rev. Mod. Phys.* **75**, 543 (2003).
- [23] J. J. Larsen, K. Hald, N. Bjerre, H. Stapelfeldt, and T. Seideman, *Phys. Rev. Lett.* **85**, 2470 (2000).
- [24] J. Itatani *et al.*, *Nature (London)* **432**, 867 (2004).
- [25] R. A. Bartels, T. C. Weinacht, N. Wagner, M. Baertschy, C. H. Greene, M. M. Murnane, and H. C. Kapteyn, *Phys. Rev. Lett.* **88**, 013903 (2001).
- [26] T. Kanai, S. Minemoto, and H. Sakai, *Nature (London)* **435**, 470 (2005).
- [27] J. Wu, H. Qi, and H. Zeng, *Phys. Rev. A* **77**, 053412 (2008).
- [28] H. Cai *et al.*, *Opt. Lett.* **34**, 827 (2009).
- [29] J. Wu *et al.*, *Phys. Rev. A* **79**, 063812 (2009).
- [30] F. Calegari, C. Vozzi, S. Gasilov, E. Benedetti, G. Sansone, M. Nisoli, S. De Silvestri, and S. Stagira, *Phys. Rev. Lett.* **100**, 123006 (2008).
- [31] S. Varma, Y.-H. Chen, and H.-M. Milchberg, *Phys. Rev. Lett.* **101**, 205001 (2008).
- [32] J. Wu *et al.*, *Opt. Lett.* **33**, 2593 (2008).
- [33] E. T. J. Nibbering *et al.*, *J. Opt. Soc. Am. B* **14**, 650 (1997).
- [34] J. Ortigoso *et al.*, *J. Chem. Phys.* **110**, 3870 (1999).
- [35] K. Mishima, M. Hayashi, J. Yi, S. H. Lin, H. L. Selzle, and E. W. Schlag, *Phys. Rev. A* **66**, 033401 (2002).
- [36] A. Mysyrowicz *et al.*, *New J. Phys.* **10**, 025023 (2008).
- [37] C. P. Hauri *et al.*, *Appl. Phys. B: Lasers Opt.* **79**, 673 (2004).
- [38] A. Zair *et al.*, *Opt. Express* **15**, 5394 (2007).
- [39] W. Lei *et al.*, *Opt. Lett.* **34**, 166 (2009).
- [40] A. Couairon, *Eur. Phys. J. D* **27**, 159 (2003).
- [41] A. Couairon *et al.*, *Opt. Lett.* **30**, 2657 (2005).
- [42] M. A. Porras, A. Parola, D. Faccio, A. Couairon, and P. Di Trapani, *Phys. Rev. A* **76**, 011803(R) (2007).
- [43] K. D. Moll, A. L. Gaeta, and G. Fibich, *Phys. Rev. Lett.* **90**, 203902 (2003).
- [44] S. Wen and D. Fan, *J. Opt. Soc. Am. B* **19**, 1653 (2002).
- [45] A. C. Bernstein, M. McCormick, G. M. Dyer, J. C. Sanders, and T. Ditmire, *Phys. Rev. Lett.* **102**, 123902 (2009).
- [46] B. Prade *et al.*, *Opt. Lett.* **31**, 2601 (2006).
- [47] C. Ruiz, J. S. Roman, C. Mendez, V. Diaz, L. Plaja, I. Arias, and L. Roso, *Phys. Rev. Lett.* **95**, 053905 (2005).